HHS Public Access

Author manuscript

ACS Nano. Author manuscript; available in PMC 2019 February 27.

Published in final edited form as:

ACS Nano. 2018 April 24; 12(4): 3714–3725. doi:10.1021/acsnano.8b00940.

Prostate-Specific Membrane Antigen Targeted Gold Nanoparticles for Theranostics of Prostate Cancer

Joey Dacula Mangadlao[†,⊥], **Xinning Wang**[†,‡,⊥], **Christopher McCleese**[§], **Maria Escamilla**[§], **Gopalakrishnan Ramamurthy**[†], **Ziying Wang**[†], **Mukul Govande**[†], **James P. Basilion**[*,†,‡], and **Clemens Burda**[*,§]

[†]Department of Radiology, Case Western Reserve University, Cleveland, Ohio 44106, United States

[‡]Department of Biomedical Engineering, Case Western Reserve University, Cleveland, Ohio 44106, United States

[§]Department of Chemistry, Case Western Reserve University, Cleveland, Ohio 44106, United States

Abstract

Prostate cancer is one of the most common cancers and among the leading causes of cancer deaths in the United States. Men diagnosed with the disease typically undergo radical prostatectomy, which often results in incontinence and impotence. Recurrence of the disease is often experienced by most patients with incomplete prostatectomy during surgery. Hence, the development of a technique that will enable surgeons to achieve a more precise prostatectomy remains an open challenge. In this contribution, we report a theranostic agent (AuNP-5kPEG-PSMA-1-Pc4) based on prostate-specific membrane antigen (PSMA-1)-targeted gold nanoparticles (AuNPs) loaded with a fluorescent photodynamic therapy (PDT) drug, Pc4. The fabricated nanoparticles are well-characterized by spectroscopic and imaging techniques and are found to be stable over a wide range of solvents, buffers, and media. *In vitro* cellular uptake experiments demonstrated significantly higher nanoparticle uptake in PSMA-positive PC3pip cells than in PSMA-negative PC3flu cells. Further, more complete cell killing was observed in Pc3pip than in PC3flu cells upon exposure to light at different doses, demonstrating active targeting followed by Pc4 delivery. Likewise, *in vivo* studies showed remission on PSMA-expressing tumors 14 days post-PDT. Atomic absorption spectroscopy revealed that targeted AuNPs accumulate 4-fold higher in PC3pip than in PC3flu tumors. The nanoparticle system described herein is envisioned to provide surgical guidance for prostate tumor resection and therapeutic intervention when surgery is insufficient.

[*]**Corresponding Authors:** cxb77@case.edu. jxb206@case.edu.

[⊥]Author Contributions

J. D. Mangadlao and X. Wang contributed equally to this work.

Supporting Information

The Supporting Information is available free of charge on the ACS Publications website at DOI: 10.1021/acsnano.8b00940. HPLC chromatograms for the purification of the peptide and conjugates, TEM image of AuNP-DDA, size distribution of AuNP DDA synthesized in different batches, results of the stability studies, representative DLS graph, summary of the singlet oxygen generation experiments, release studies in media and in blood, and mechanism of DCFDA detection of ROS (PDF)

The authors declare no competing financial interest.

Graphical Abstract

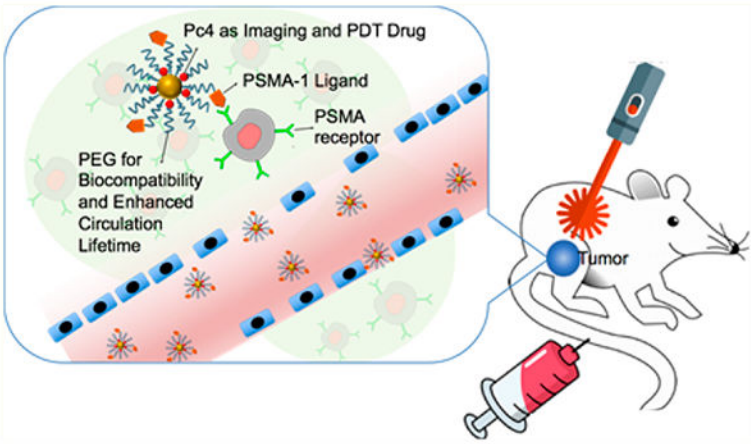

Keywords

prostate cancer; PSMA; gold nanoparticles; photodynamic therapy; theranostics

Prostate cancer is the most prevalent cancer and is the third leading cause of cancer deaths in men in the United States.[1] Approximately 161 000 diagnoses and 26 730 deaths are projected in 2017 among American males. Roughly 91% of men diagnosed with the disease at initial screenings have clinically localized tumors and are candidates for radical prostatectomies, or the surgical removal of the prostate gland.[2] However, during surgery, cancer has been shown to extend outside the prostate in 20−42% of patients, resulting in the failure to achieve a surgical cure in patients who underwent radical prostatectomy.[3] In addition, surgical approaches to prostate cancer are largely associated with significant morbidity such as incontinence (3−74%) and impotence (30−90%).[4–7] Hence, the development of a technology that will improve the success rate for prostatectomies and simultaneously reduce surgery-related morbidities in localized cancers is not only an open challenge but also an urgent necessity.

Thanks to modern molecular biology, prostate-specific membrane antigen (PSMA) was identified to differentiate benign from malignant disease, enabling the development of potential targets for treatment strategies.[8] PSMA is a type II transmembrane protein composed of 750 amino acid residues with a molecular weight of 110 kDa. It is overexpressed in all cases of prostate adenocarcinoma and in the neovasculature of solid tumors such as colon, breast, and lung carcinomas.[9] More importantly, the cytoplasmic tail of PSMA has an internalization motif suggesting that therapeutics with PSMA ligands are internalized into the cell.[10,11]

In this study, we developed a nanoparticle-based platform to target prostate cancer tumors for the delivery of a fluorescent and photodynamic therapy (PDT) drug, Pc4 (Scheme 1). A brief overview of the mechanism of PDT can be found in the Supporting Information, and a thorough review is discussed elsewhere.[12] Eventually, we foresee this technology to potentially improve the success rate for prostatectomies and simultaneously reduce surgery-

related morbidities in localized cancers. Using a mouse model as the first step in accomplishing this goal, we built upon our expertise with molecular imaging and nanoparticle drug delivery to develop theranostic nanoparticles that will potentially permit image-guided removal of cancer tissues and provide the added benefit of allowing ablation of diseased tissues that are unable to be resected. As a proof of concept, an animal model bearing heterotopically implanted prostate cancer tumor was utilized to ascertain the feasibility of the proposed approach.

Ideally, a good PDT agent should have high absorption maxima at wavelengths longer than 630 nm (tissue penetration of light is optimal at the red region of the electromagnetic spectrum), have a high extinction coefficient, have high quantum yield of $^1O_2$, and have good water solubility. Phthalocyanine-based Pc4 [HOSiPcOSi$(CH_3)_2(CH_2)_3$N-$(CH_3)_2$] has been our mainstay PDT drug not only because it is already approved for clinical trials[13] but also because it possesses those aforementioned characteristics, except that it is insoluble in aqueous systems. To circumvent this dilemma, we have recently developed covalent synthetic routes using Pc4 derivatives to render the molecule water-soluble.[14] In the past, we have also developed a noncovalent nanoparticle-based Pc4 delivery platform for brain cancer.[15–18] Apart from eliminating tedious synthetic modifications, the noncovalent approach ensures the delivery of the drug in its native form. With nanoparticles as delivery vehicle, we are able to exploit the enhanced permeation retention (EPR) effect, which allows particles of a certain size to have a longer residence time in the tumor as a consequence of the tumor's leaky vasculature and poor lymphatic drainage.[19–21] Hence by EPR, drug-loaded nanoparticles passively accumulate in the tumor where the noncovalently encapsulated payload can be released and be concentrated. However, recent studies suggest that delivery of nanodrugs by virtue of EPR alone offers a less than 2-fold increase in drug delivery, resulting in concentrations that are insufficient for curing most cancers.[22] On the other hand, active targeting, *i.e.*, nanoparticles functionalized with ligands specific to disease biomarkers, increases the affinity of the nanoparticles for tumor cells, resulting in increased tumor residence times and internalization by receptor-mediated endocytosis.[23,24]

There exist few reports on PSMA-targeted nanoparticles. "Soft" materials based on architectured polymeric nanostructures, such as poly(lactic acid)−polyethyene glycol (PLA-PEG) nanoparticles,[25,26] PEG-cholesterol micelles,[27] and aliphatic hyperbranched polyester,[28] and "hard" materials such as multiwalled carbon nanotubes[29] and superparamagnetic iron oxide nanoparticles[30] have been functionalized with PSMA ligands for imaging, drug delivery, and other therapeutic applications. Recently, gold nanoparticle conjugated anti-PSMA antibody was developed to spectroscopically detect prostatic disease based on localized surface plasmon resonance (LSPR) of gold nanoparticles.[31] In this contribution, we report the synthesis, characterization, and application of thoroughly characterized PSMA-1-targeted gold nanoparticles for the theranostics of prostate cancer. PSMA-1 ligand was first conjugated to thiol-terminated polyethylene glycol (PEG), which was then subsequently grafted to the AuNP surface by ligand-exchange reaction. The efficacy of these nanoparticles against PC3pip (PSMA+) and PC3flu (PSMA−) cells was evaluated *In vitro* and *in vivo* (Scheme S1). For *in vivo* studies, PC3pip and PC3flu cells were heterotopically implanted into the right and left flanks of nude athymic mice, respectively. When the tumors were of sufficient size, the nanodrug was introduced to the animal *via* tail-vein injection.

Preferential binding to PSMA-expressing tumor was evaluated using a whole animal *in vivo* fluorescence Maestro imaging system and by analyzing the gold content of the tumors *ex vivo* by atomic absorption spectrometry (AAS). PDT experiments were then performed by irradiating the tumor area with a 672 nm laser diode. The animals were then monitored for 14 days post-PDT, and measurements such as tumor volume and total body weight were recorded. Overall, the results of the experiments conducted indicate that PSMA-1-targeted AuNPs are a vector to deliver Pc4 for the theranostics of prostate cancer. This can be potentially translated into surgical applications such as intraoperative imaging for real-time assessment of the extent of invasion, image-guided surgery for precise differentiation between compromised and healthy tissues, and PDT ablation to guarantee maximum removal of cancer after conventional prostatectomy.

RESULTS AND DISCUSSION

PSMA-1 is a urea-based ligand routinely synthesized in our laboratory using standard fluorenylmethyloxycarbonyl chemistry. We have previously shown that PSMA-1 demonstrated enhanced binding affinity (IC_{50} = 2.30 nM) to the PSMA receptor compared to its parent ligand Cys-CO-Glu (IC_{50} =9.93 nM).[32] The lysine residue at the C-terminus offers the opportunity to conjugate biologically relevant molecules such as compatibilizers, drugs, and imaging agents through a myriad of available amine chemistry. In this study, we utilized a 5 kDa bifunctional PEG-containing orthopyridyl disulfide (OPSS) terminal group on one end and N-hydroxysuccinimide (NHS) ester on the other. PEGylation was performed *via* standard carbodiimide cross-linking chemistry to couple the NHS ester to the lysine N of the C-terminus of PSMA-1 (Figure 1a). The synthesized materials were purified by high-performance liquid chromatography (HPLC), where the UV absorbance of the OPSS group was instrumental in monitoring the successful conjugation of PSMA-1 ligand and PEG. We employed MALDI-TOF MS to confirm the mass of the synthesized conjugates as shown in Figure 1b and Figure S1. After conjugation, an approximately 1 kDa shift in the mass spectra of SH-5kPEG-PSMA-1 evidenced the successful coupling of the 1087 Da PSMA-1 and the 5 kDa OPSS-5kPEG-NHS.

Dodecylamine (DDA)-stabilized gold nanoparticles (AuNPDDA) were then synthesized using the modified Brust− Schiffrin method.[16] A representative transmission electron microscopy (TEM) image of AuNP-DDA is displayed in Figure S2. We synthesized three batches of AuNP-DDA and performed TEM and UV−vis analyses to ascertain consistency in the fabrication of the nanoparticles. Figure S3 shows that based on the size distribution and spectral profile our synthesis of precursor AuNP-DDA is consistent and reproducible. In order to graft the PSMA-1 ligand onto the nanoparticle, a ligand-exchange reaction was performed by virtue of the strong interaction between gold and thiol. Briefly, a 1000 molar excess of SH-5kPEG-PSMA-1 and SH-5kPEG ligands in 1:5 molar ratio was allowed to react with 1 equiv of AuNP-DDA for 2 days (Figure 2a). Excess ligands and other reaction products were removed by extensive purification using centrifuge filters (MWCO = 50 kDa) followed by freeze-drying. The complete removal of free ligands is critical to avoid competitive binding between the nanoparticle and the unbound ligand to the PSMA receptor. Hence, the filtrate was also collected, freeze-dried, and weighed at each purification cycle to confirm complete removal. We found that roughly 60% of the loaded ligands were in excess,

suggesting that approximately 40% were successfully grafted on the nanoparticle (Figure S4). To demonstrate successful attachment of the PSMA-1 ligand to the nanoparticle, agarose gel electrophoresis experiments were performed in TAE buffer at pH 8.3 (Figure 2b). Being highly negatively charged due to abundant glutamic acid residues, PSMA-1-targeted gold nanoparticles migrated to the anode, suggesting that the nanoparticle surface is well-functionalized with the peptide. In contrast, nontargeted gold nanoparticles migrated to the cathode together with the electroosmostic flow tracer, vitamin B12. This is consistent with our previous report detailing the electrophoretic mobilities of PEGylated gold nanoparticles.[33]

It is well-known that PEG is beneficial in enhancing the solubility, reducing nonspecific binding, improving biocompatibility, and increasing the circulation half-life of small-molecule and nanoparticle-based drugs.[34] Furthermore, PEG's amphiphilicity allows the encapsulation of water-insoluble Pc4 in the corona of the nanoparticle. Pc4 loading was performed by adding a 40-fold excess of Pc4 to a AuNP-5kPEG-PSMA-1 solution in chloroform. Due to the amphiphilic nature of PEG, chloroform swells the corona, which facilitates the diffusion of Pc4 molecules into the PEG coating. After incubation for 48 h, the solvent was removed and final AuNP-5kPEG-PSMA-1-Pc4 conjugates were purified through a 0.25 μm syringe filter. Thorough characterization involving spectroscopic and imaging techniques was performed to fully understand the nature of the synthesized nanoparticle conjugates. We utilized UV−vis spectroscopy (Figure 2c) and the signature LSPR band of AuNPs at 520 nm and the absorbance of Pc4 at 670 nm to calculate the loading of the latter. We found an average of ~20 molecules of Pc4 per AuNP. It is worth mentioning that the absorbance of encapsulated Pc4 bathochromically shifted from 670 to 680 nm. The 10 nm shift is due to the electronic effects brought about by the gold and PEG environment, which is also an indication that the Pc4 molecules are actually trapped inside the polymeric shell. Reports have also shown that phthalocya-nines have the tendency to aggregate at high concentrations and in poor-solvent environments, resulting in a red-shift in its absorption spectra.[35,36] These conditions are possible in these AuNP-Pc4 conjugates in aqueous solution. However, the Pc4 molecules are unlikely to aggregate in the polymer shell, since no spectroscopic signatures of H- and J-aggregates were identified.

The advantages of nanosized drugs for cancer diagnosis and treatment include their ability to have large loading capacity, their ability to protect the payload from degradation, a large surface area to volume ratio allowing a variety of targeting ligands to be grafted, and the amenability for controlled or sustained release.[22] Due to EPR effect, nanosized drugs preferentially penetrate the tumor tissues through leaky vasculature and are retained in the tumor bed due to poor lymphatic drainage. The EPR effect is a size- and time-dependent process; therefore it is critical that formulated drug-loaded nanocarriers are stable over a suitable period of time. We utilized UV−vis spectroscopy to monitor the stability of AuNP conjugates at room temperature in biologically relevant buffers and media such as RPMI + 10% FBS, PBS, TBS, citrate buffer, NSS, and water at pH 7, 3, and 10 (Figure S5). We found that the conjugates in solution are stable in most solvents for at least three months. More importantly, the stability in media (RPMI + 10% FBS) is noteworthy because unlike small-molecule drugs, nanosized drugs slowly leak from the blood vessels after intravenous introduction. Hence, the accumulation of drugs into the tumor would be inadequate if the

nanosized drugs were unstable in the serum.[37] We also monitored the potential aggregation of the nanoparticles by examining them using TEM. Figure 3a demonstrates that PEGylated nanoparticles present a nearly unimodal distribution centered at 5.5 ± 0.4 nm. To visualize the shell or the corona of the nanoparticle, the sample was stained with 2% phosphotungstic acid (PTA) prior to imaging (Figure 3b). The overall size of the nanoparticle (Au core + corona) is 23 ± 3 nm. In contrast, we found that the size as determined by dynamic light scattering (DLS) is 26.5 ± 1.1 nm, which is expected, as DLS measures the hydrodynamic size, taking into account the interaction of the material with the solvent (Figure S6). Long-term stability was tested by storing the particles at −20 °C followed by TEM imaging a year later (Figure 3d). Interestingly, the corona is intact although the overall size decreased to 17 ± 2 nm. To gain further understanding about this phenomenon, we re-examined the UV−vis absorbance of the nanoparticle by dispersing it in water (Figure 3d). The nanoparticles instantaneously dispersed in solution, suggesting that the nanoparticles are not agglomerated and are in fact stable. Furthermore, the spectral profile of the year-old nanoparticle solution overlays that of the previous. This is an interesting finding, suggesting that the grafted polymer rearranges to a more compact structure over time. Being a crystalline polymer with a narrow polydispersity, the PEG chains over time at low temperature are likely to rearrange into a dense and compact shell surrounding the nanoparticle.[38]

The tenet of photodynamic therapy is the ability of the PDT agent to generate reactive oxygen species (ROS), mainly singlet oxygen ($^1O_2$), when activated by light. These generated products are highly reactive and can oxidize key cellular components, leading to tumor ablation. In order to confirm the ability of Pc4 to generate $^1O_2$, we performed the photo-irradiation of Pc4 in the presence of a $^1O_2$ trap, diphenylisobenzofuran (DPBF). When $^1O_2$ is generated, DPBF photodecomposes, which can be conveniently monitored by UV−vis absorption at 410 nm. Figure 4a shows the decomposition of DPBF in the presence of irradiated Pc4 over time, suggesting concomitant production of cytotoxic $^1O_2$. The results of our $^1O_2$ experiments are summarized in Figure S7, showing the response at different solvents (ethanol, PBS, and media), Pc4 concentration, and light dosage. Generally, increasing the concentration and dosage led to rapid decomposition of DPBF, hence rapid generation of $^1O_2$. It is worth noting that we performed the experiment in media to determine if $^1O_2$ will be generated in a biological environment. More importantly, we evaluated the generation of $^1O_2$ species of the as-synthesized AuNP conjugates (Figure 4b). We compared the performance of AuNP-5kPEG-PSMA-1-Pc4 against physically mixed Pc4 and AuNP-5kPEG. As shown in Figure 4b, the presence of Pc4 is essential in the generation of $^1O_2$ species, as physically mixed DPBF and AuNP alone did not exhibit an appreciable decrease in absorbance (the slight increase is due to solvent evaporation). The absorbance of physically mixed DPBF + Pc4 decreased to 31.5 ± 6.8%, while that of physically mixed DPBF + AuNP-5kPEG + Pc4 decreased to 46.6 ± 2.9%. This is anticipated since physically mixed Pc4 can freely interact with DPBF in solution, resulting in the rapid generation of $^1O_2$. The difference of the performance of the physically mixed system with and without AuNP may well be due to the slight absorbance of AuNP at 678 nm. In contrast, the absorbance of AuNP-5kPEG-PSMA-1-Pc4 minimally decreased to 85.1 ± 5.4%, a compelling evidence that the Pc4 drugs are encapsulated within the corona of the

nanoparticle and protected from light activation. This feature is essential to minimize premature and nonspecific release of the drug during introduction.

We have previously shown that targeted interaction of the loaded nanoparticle with the cell initiates transfer of the hydrophobic payload to hydrophobic regions within the cell (e.g., mitochondrial and cellular membranes).[15,16,18,24] To mimic this, we performed a drug release study in a two-phase system composed of AuNP conjugates either in media or in mouse blood as the aqueous layer and toluene as the hydrophobic component. Figure S8 and Figure S9 indicate that these hydrophobic Pc4 molecules can be released into an adjacent hydrophobic environment.

The apparent affinity of the PSMA-targeted nanoparticle was then evaluated by competition binding assay to determine the IC_{50} (Figure 5a). PSMA-expressing PC3pip cells were incubated with different concentrations of AuNP-5kPEGPSMA-1, PSMA-1, and the parent ligand, ZJ24, in the presence of 12 nM ^{3}H-labeled ZJ24. Cell-associated uptake was determined by measuring the radioactivity *via* a scintillation counter. Compared to ZJ24 (IC_{50} = 9.66 nM) and PSMA-1 (IC_{50} = 2.01 nM) ligands, AuNP-5kPEG-PSMA-1 remarkably exhibited the lowest IC_{50} value (IC_{50} = 0.17 nM). The 12-fold increase in binding avidity as compared to PSMA-1 is likely due to the multiple PSMA-1 ligands in each nanoparticle. Multivalency has been shown to enhance binding to the desired target and a key factor to improve biological targeting.[39,40] Similar to dendrimers studied by Hong *et al*,[39] the spherical geometry of AuNPs preorganizes the ligands into a small region of space, which limits their degree of freedom as compared to the free peptide, PSMA-1. This compensates for the entropic penalty required for localizing the targeting ligands into the tumor. Due to the directionality offered by thiol−gold interaction, our synthetic design to have PSMA-1 on one end and thiol on the other ensures that PSMA-1 ligands are exposed to the surface of the nanoparticle and allows all targeting to address the cell surface.

Next, the *In vitro* phototoxicity of Pc4-bearing targeted and nontargeted AuNP conjugates was determined (Figure 5b). PSMA-expressing PC3pip or nonexpressing PC3flu cells were incubated with Pc4-containing nanoparticles for 4 h. Following washing, the cells were exposed to different doses of light (0, 0.1, 0.5, and 1 J), and the percentage of surviving cells was calculated 24 h later using a 3-(4,5-dimethylthiazol-2-yl)-5-(3-carboxymethoxyphenyl)-2-(4-sulfophenyl)-2*H*-tetrazolium (MTS) assay. Figure 5b shows that at 1 J, PSMA-targeted AuNPs killed approximately 8 times more PC3pip (4.9 ± 2.2%) than PC3flu cells (37.1 ± 7.7%). To a certain extent, nontargeted gold nanoparticles can kill PC3pip and PC3flu cells at elevated irradiation doses, which may be due to nonspecific release and absorption of free Pc4 into the cells. These results show that AuNP-5kPEG-PSMA-1-Pc4 conjugates are more efficient at killing PSMA-expressing cells than nontargeted nanoparticles. They are more selective for PSMA-expressing cells, which evidenced active targeting and Pc4 delivery to cells as a result of conjugating the AuNPs with the PSMA-1 ligand. To further probe the mechanism of toxicity, we performed an intracellular ROS assay. PC3pip cells were incubated with dichlorofluorescein diacetate (DCFDA) and then treated with either targeted or nontargeted gold nanoparticles containing Pc4. When free radicals are generated within the cells, the nonfluorescent DCFDA is converted to fluorescent 2′,7′-dichlorofluorescein (DCF^{-}) as it reacts with cellular ROS

(λ_{Ex} = 495 nm; λ_{Em} = 529 nm).[41] The mechanism of the transformation is shown in Figure S10. The assay was performed by incubating PC3pip cells with targeted and nontargeted gold nanoparticles together with DCFDA followed by irradiation. Figure 5c displays the fluorescence images of the cells at the corresponding emission windows of each fluorophore (nucleus was stained with 2-(4-amidinophenyl)-6-indolecarbamidine dihydrochloride, DAPI). The data show that cells treated with AuNP5kPEG-PSMA-1-Pc4 exhibited more fluorescence signal, suggesting Pc4 results in production of ROS. This result further confirms the efficient delivery of Pc4 as a result of PSMA targeting.

The PSMA receptor has an internalization motif MXXXL and is reported to have a robust baseline internalization rate of 60% of its surface PSMA in 2 h, suggesting that PSMA-1-targeted AuNPs are internalized *via* clathrin-mediated endocytosis.[11] To this end, we performed silver staining to ascertain whether the AuNPs are within the cellular milieu. In this procedure, silver ions nucleate around gold nanoparticles and precipitate as silver metal. The silver-coated gold further catalyzes more silver deposition, resulting in particle growth, hence the visibility under a light microscope. It is evident in Figure 6 that there is significantly higher gold uptake in PSMA-expressing PC3pip cells than in PSMA-negative PC3flu cells. Untargeted AuNPs had significantly less uptake by PSMA-expressing cells, similar to the level of uptake measured with cells not expressing PSMA. As shown in Figure 6, the uptake of Pc4 correlated well with the cell-associated AuNP assessed by silver staining.

Establishing that AuNP5kPEG-PSMA-1 is effective at targeting and delivering Pc4 to cells *In vitro*, we next studied the efficacy of the AuNP conjugates *in vivo*. Athymic nude mice were subcutaneously inoculated with 1×10^6 PC3pip or PC3flu cells in right and left flanks, respectively. When tumors were of sufficient size, the animals were injected with 0.07 mg/kg (with respect to Pc4) AuNP5kPEGPSMA-1-Pc4 *via* the tail vein. Maestro *in vivo* fluorescence imaging was used to track the fluorescence of Pc4. Figure 7a shows that Pc4 accumulates more into PSMA-expressing tumor and the release of Pc4 peaks and plateaus after 3 h postinjection (Figure S11). Typically, passive accumulation of nanoparticles into the tumor by the EPR effect takes 16−24 h. In contrast, the onset of accumulation observed in our experiment is rather immediate. In addition, the Pc4 signal also persisted up to 24 h, although there is an indication that it is gradually cleared from the tumor. These observations are consistent with active targeting due to PSMA. Although it may appear from Figure S11 that there seems to be little improvement due to targeting, we hypothesized that the fluorescence of Pc4 was quenched due to the presence of AuNP in the PC3pip tumor. Hence, to determine gold content, we excised both pip and flu tumors after 3 h and performed acid digestion. By AAS, we found that AuNP5kPEG-PSMA-1-Pc4 accumulates 4× more in PC3pip than in PC3flu tumors (Figure 7c). We also sectioned the tumor tissues and performed a quick silver stain to qualitatively determine which tissue had more gold content. Figure 7c (inset) shows that thin sections of PC3pip tumor turned dark while PC3flu showed little to no darkening after silver staining. All these results clearly demonstrate active targeting and delivery of Pc4 as a result of PSMA-1 conjugation.

As a last step in these studies we performed *in vivo* PDT experiments with mice bearing a PC3pip tumor labeled with green fluorescent protein (GFP). The efficacy of the treatment

was evaluated by monitoring tumor growth using a digital caliper, GFP fluorescence by Maestro, and body weight loss for 14 days post-PDT. At 3 h postinjection of the AuNP5kPEGPSMA-1-Pc4, the tumor was irradiated with 672 nm light at a constant fluence rate of 0.1 W/cm^2 for 25 min (150 J/cm^2) and 50 min (300 J/cm^2). Immediate swelling following PDT is typically seen in PDT studies, but usually resolves in 3 days. In addition, no toxicity to the animals was noted other than scabbing at the irradiation site, which also disappears in a few days. Figure 8a shows the black and white and corresponding GFP fluorescence images of the same mouse monitored over time, indicating that the tumor is decreasing in size and fluorescence intensity.

Figure 8b–d show the efficacy of the treatment, especially at a higher dosage of light. The group treated with 300 J/cm^2 was in remission 14 days post-treatment and was generally healthier and active, as also evidenced by their weight gain.

The findings presented indicate that PSMA-targeted gold nanoparticles can be utilized to selectively target prostate cancer *In vitro* and *in vivo*. More importantly, these nano-particles can efficiently deliver the imaging and PDT agent Pc4, selectively to PSMA-expressing prostatic disease. By delivering Pc4 directly to prostate cancer cells, potential applications, such as (1) intraoperative imaging to assess extracapsular invasion of the prostate cancer and inform real-time intraoperative decision making; (2) intraoperative image-guided resection of prostate cancer and differentiation of critical surrounding structures (*e.g.*, nerve bundles and urethral sphincter); and (3) PDT ablation of nonresectable tumor tissues to ensure maximum removal of cancer after conventional surgery is completed, are accessible and will be explored in the future.

SUMMARY AND CONCLUSION

Stable PSMA-targeted gold nanoparticles were synthesized and extensively characterized by spectroscopic and imaging techniques. The theranostic gold nanoparticle was engineered to contain and deliver Pc4, which is both an imaging agent and a potent anticancer PDT drug. These nanoparticles have a highly effective mechanism to deliver drugs to prostate cancer cells *In vitro* and *in vivo*. Results of *In vitro* cellular uptake experiments demonstrated significantly higher nanoparticle uptake in PSMA+ PC3pip cells than in PSMA− PC3flu cells. In addition, more cell ablation was observed in PC3pip than in PC3flu cells upon exposure to light at different doses, demonstrating active targeting followed by Pc4 delivery. *In vivo*, we have demonstrated that these nanoparticles can selectively deliver the payload that allows visualization of the tumor and enables their destruction when they are irradiated with light. Treated animals showed remission of the tumor 14 days post-PDT, demonstrating that PSMA-targeted gold nanoparticles are effective materials in providing surgical guidance for prostate tumor resection and therapeutic intervention when surgery is insufficient.

METHODOLOGY

Synthesis of Glu-CO-Glu′-Amc-Ahx-Glu-Glu-Glu-Lys-NH_2 (PSMA-1).

Using standard fluorenylmethyloxycarbonyl (Fmoc) chemistry, the peptide was synthesized at 0.2 mmol scale starting from C-terminal Fmoc-rink amide 4-methylbenzhydrylamine

resin. A 20% piperidine in dimethylformamide (DMF) solution was used during every Fmoc deprotection cycle. Ninhydrin test was also performed at each addition cycle. The coupling of the amino acids was carried out using 3.3 equiv of Fmoc amino acids in DMF activated with 3.3 equiv of 2-(6-chloro-1-*H*-benzotriazole-1-yl)-1,1,3,3-tetramethylaminium hexafluorophosphate and 5 equiv of diisopropylethylamine (DIPEA) in DMF. After the peptide sequence Fmoc-Glu′-Amc-Ahx-Glu-Glu-Glu-Lys(Mtt) was assembled on the resin, the Fmoc group of N-terminal amino acid Glu′ was deprotected by 20% piperidine. The Amc, Ahx, and Lys(Mtt) residues are from *trans*-4-(9-fluorenylmethyloxycarbonylaminomethyl)cyclohexanoic acid, 6-(Fmoc-amino)hexanoic acid, and *N*-α-Fmoc-*N*-ε−4-methyltrityl-L-lysine, respectively. Then, a chloroform solution containing 3 equiv of H-Glu(OtBu)-OtBu mixed with 2.5 equiv of DIPEA was then prepared followed by its slow addition to 0.25 equiv of triphosgene in chloroform over 10 min at RT. After a 15 min reaction, the mixture was mixed with Glu′-Amc-Ahx-Glu-Glu-Glu-Lys on the resin preswollen in chloroform with 2.5 equiv of DIPEA. After the reaction, the resin was washed with DMF and then dichloromethane and dried overnight. The peptide was released from the resin using trifluoroacetic acid/water/triisopropylsilane (95%:2.5%:2.5%). The purification of the cleaved peptide was performed using preparative HPLC. The products were characterized by high-resolution matrix-assisted laser desorption/ionization −time-of-flight mass spectroscopy (MALDITOF MS) using Bruker AutoFlex III MALDI-TOF-TOF MS in the positive ion mode. The retention time was 18.6 min. MALDI-MS: $C_{48}H_{74}N_{10}O_{20}$, 1087.5 (found); 1087.1 (calculated).

Synthesis of SH-5kPEG-PSMA-1.

The PEGylation of PSMA-1 was performed through the γ-NH_2 of lysine. PSMA-1 (1 mg) was dissolved in 200 μL of PBS, and Et_3N was added until the pH was between 7 and 8. Then, a 2-fold excess of NHS-5kPEG-OPSS (Jenkem Technology) predissolved in 200 μL of DMF was mixed with the PSMA-1 solution. The mixture was allowed to react overnight in a rotary mixer. Purification through HPLC was then performed. For deprotection, a 10-fold excess of tris(2-carboxyethyl)phosphine was added to OPSS-5kPEG-PSMA-1 to reduce the OPSS groups to corresponding thiol (−SH) groups. The reaction was performed in H_2O and was carried out for 2 h followed by dialysis (MWCO = 2 kDa) against deionized H_2O overnight. The dialyzed material was lyophilized, and successful removal of the OPSS group was confirmed by HPLC.

Synthesis of Gold Nanoparticle Conjugates.

The gold nanoparticles were prepared by first mixing 0.1367 g of tetraoctylammonium bromide and 5 mL of toluene. After 5 min of mixing, 367 μL of gold(III) solution (30 wt % in dilute HCl) was added, and the mixture was allowed to stir for 5 min. DDA (0.112 g) was then added to the solution. Following another 10 min of stirring, 1 mL of a 0.0756 g/mL sodium borohydride ($NaBH_4$) ice-cold water solution was added slowly at 50 μL/15 s increments. The addition of $NaBH_4$ will immediately turn the color of the solution from salmon orange to wine red. The reaction mixture was allowed to stir for 2 h. To precipitate AuNP-DDA, the mixture was poured into 50 mL of 100% ethanol for 15 min at 4000 rpm. The supernatant was decanted followed by another round of ethanol washing. The AuNP-DDA nanoparticles were then dried under a stream of N_2 gas for 30 min. Then, the dried

nanoparticles were dissolve in 5 mL of chloroform ($CHCl_3$) followed by centrifugation at 4000 rpm for 15 min. Only the supernatant was collected. The concentration was determined by UV−vis spectroscopy based on gold's LSPR absorption band at 520 nm ($\varepsilon = 2.737 \times 10^7$ L/mol/cm). To synthesize AuNP-5kPEG-PSMA-1, a 1000 molar excess of SH-5kPEG-PSMA-1 and SH-5kPEG ligands in 1:5 molar ratio was allowed to react with 1 equiv of AuNP-DDA for 2 days. Excess ligands and other reaction products were removed by extensive purification using centrifuge filters (MWCO = 50 kDa) followed by freeze-drying. In order to fabricate AuNP-5kPEG-PSMA-1-Pc4, a 40-fold excess of Pc4 was added to a AuNP-5kPEG-PSMA-1 solution in chloroform. After incubation for 48 h, the solvent was removed and final AuNP-5kPEG-PSMA-1-Pc4 conjugates were purified through a 0.25 μm syringe filter.

Characterization of Gold Nanoparticle Conjugates.

All UV− vis spectroscopy studies were performed on a Tecan Infinite M200. In a typical experiment, the absorbance of AuNP conjugates dissolved in a solvent of choice was collected from 300 to 800 nm, paying attention to the AuNP's LSPR band at 520 nm and Pc4's Q-band at 670 nm. For stability studies in solution, stock solutions of AuNP conjugates in media (RPMI + 10% FBS), DI H_2O (at pH 3, 7, and 10), PBS, TBS, NSS, and citrate and RIPA buffer were prepared and were stored at room temperature. The absorbance of these solutions was monitored in triplicates at 520 and 670 nm at certain time points by pipetting out 200 μL of the stock solution into a 96-well plate array. A ZetaPALS dynamic light scattering system (Brookhaven Instruments) was used to determine the hydrodynamic size of the nanoparticle conjugates. For absolute size determination, a sample was dropped onto 400 mesh copper TEM grids with a Formvar/carbon support (Ted Pella, Inc.). Prior to staining, excess sample was wicked off the TEM grid with filter paper. Then, 2% PTA was dropped onto the grid, again wicking off the excess with filter paper. The grid was allowed to dry at RT overnight, and imaging was performed on a FEI Tecnai 12 Spirit TEM operating at 100 kV accelerating voltage. On the other hand, gel electrophoresis studies were performed on a 1% agarose gel and 1× TAE running buffer. Each sample consisted of 10 μL of 2 mM AuNP conjugates, 5 μL of glycerol, and 5 μL of water. An electroosmostic flow tracer, vitamin B12, was also included. The gel was run at 120 V for 30 min.

Singlet Oxygen Generation Experiments.

The singlet oxygen generation was determined by the decomposition of DPBF (50−200 mM) in the presence of free or encapsulated Pc4 (10 mM). The experiment was performed in ethanol, PBS, or media (RPMI + 10% FBS). In a typical experiment, 100 mL of DPBF solution was mixed with 10 mL of Pc4 solution in a 96-well plate. The well was then irradiated with 1−5 mW/cm^2 of 672 nm light from a diode laser (Applied Optronics Corp.) equipped with a GRIN-lens-terminated multimode fiber (OZ Optics). Every 10 s, the decay of DPBF was monitored by its absorption at 410 nm using a Tecan Infinite M200 plate reader.

Cell Culture.

Retrovirally transfected PSMA+ PC3pip cells and PSMA− PC3flu cells obtained from Dr. Michel Sadelain in 2000 (Laboratory of Gene Transfer and Gene Expression, Gene Transfer

and Somatic Cell Engineering Facility, Memorial-Sloan Kettering Cancer Center, New York, NY, USA) were used in these studies. The cells were last checked by Western blot analysis in 2017 for PSMA expression. The cells were cultured in RPMI1640 medium (Invitrogen Life Technology) with 2 mmol/L L-glutamine and 10% FBS at 37 °C and 5% CO_2 under a humidified atmosphere.

Competition Binding Assay.

The competition binding assay was carried out by incubating 5×10^5 PC3pip cells with different concentrations (1000, 100, 10, 1, 0.1 nmol) of AuNP-5kPEG-PSMA-1, PSMA-1, and ZJ24 in the presence of 12 nmol/L *N*-[*N*-[(*S*)-1,3-dicarboxypropyl]carbamoyl]-*S*-[3*H*]-methyl-L-cysteine (^{3}H-ZJ24) (GE Healthcare Life Sciences) in Tris buffer. The radioactivity of the cell pellet was counted by a scintillation counter. IC_{50}, the concentration required to inhibit 50% of binding, was determined by GraphPad Prism 3.0.

In vitro Phototoxicity by MTS Assay.

The cell viability was evaluated by the CellTiter 96 Aqueous cell proliferation assay (Promega Corporation) in the dark and under light exposure. PC3pip and PC3flu cells (1000/well) were seeded in 96-well culture plates 3 days before treatment. Then, the media was removed and replaced with 200 μL of 1 μmol/L of Pc4 in either AuNP-5kPEG-Pc4 and AuNP-5kPEG-PSMA-1-Pc4 prepared in RPMI + 10% FBS solution. After incubation for 4 h, the cells were washed twice with 200 μL of complete RPMI media, and another 200 μL of media was added prior to irradiation. The 96-well plate was then irradiated under light (>500 nm; Apollo Horizon projector, Acco Brands) with radiant exposure at 0.1, 0.5, and 1 J/cm^2. Following incubation overnight, CellTiter 96 Aqueous reagent was added to each well. After a 3 h incubation at 37 °C, the absorbance at 490 nm was measured.

In vitro Cellular Uptake Studies.

PC3pip and PC3flu cells (20 000 cells/500 μL) were plated on coverslips and were allowed to grow until about 70% confluency. The cells were then incubated with 0.5 mL of 1 μmol/L Pc4 in AuNP-5kPEG-Pc4 and AuNP5kPEGPSMA-1-Pc4 at 1, 4, and 24 h. After incubation, the cells were washed three times with PBS followed by fixing with 4% paraformaldehyde. The cells were then counterstained with DAPI and mounted with Fluor-Mount aqueous mounting solution. The slides were observed under a Leica DM4000B fluorescence microscope (Leica Microsystem Inc.). Silver staining was performed using a silver enhancer kit (Sigma-Aldrich). Following three cycles of washing with DI water, the coverslips with cells were immersed in 2 mL of a 1:1 mixture of silver salt (solution A) and initiator (solution B) for 5 min on the shaker. Following staining the silver solution was removed and the cells were washed with DI water three times. After mounting, the cells were visualized under the same microscope under light microscopy mode.

In vitro ROS Detection by DCFDA Assay.

PC3pip cells were prepared in the same manner as described above. The cells were first incubated with 20 μM DCFDA in PBS for 30 min followed by washing with PBS. Then, the cells were incubated with 1 μmol/L Pc4 in AuNP-5kPEG-Pc4 and AuNP5kPEG-PSMA-1-

Pc4 for 1 h followed by washing with PBS. After addition of fresh PBS, the cells were irradiated with 1 J/cm^2 light. The cells were then counterstained with DAPI and mounted with Fluor-Mount aqueous mounting solution. The slides were observed under a fluorescence microscope at corresponding emission windows of the fluorophores of interest.

In vivo NIR Imaging Studies.

All animal experiments were performed according to the guidelines of the Institutional Animal Care and Use Committee (IACUC #120024) at Case Western Reserve University. Six- to eight-week-old male athymic nude mice were implanted subcutaneously with 1×10^6 of PC3pip and PC3flu cells on the right and left flanks, respectively. When the tumors were of sufficient size, the Pc4-containing AuNP conjugates were injected intravenously *via* the tail vein at 0.07 mg/kg Pc4 dosage. The animals were then anesthesized with isoflurane, and fluorescence imaging was performed using the Maestro *in vivo* Imaging System (PerkinElmer) at certain time points. After imaging, the mice were euthanized, and tissues were harvested for imaging *ex vivo* and for gold content analysis. Multispectral images were unmixed into their component spectra (Pc4, autofluorescence, and background).

Gold Nanoparticle Biodistribution.

Tissue and blood samples from the injected mice (liver, lungs, heart, kidneys, skin, spleen, PC3pip and PC3flu tumors) were collected post mortem at 3 h postinjection of AuNP5kPEG-PSMA-1-Pc4. All tissue samples were stored at −20 °C, and blood samples were stored at 4 °C prior to analysis. The samples collected from each mouse were thawed, weighed, and then digested in 3 mL of aqua regia at 65 °C overnight. The digested samples were diluted up to 20 mL with deionized water and analyzed by GFAAS (Varian, SpectrAA 220 Z). Gold content was determined by calibration using a series of gold standard solutions at 242.8 nm wavelength. The data collected within each group were averaged, and standard deviations were calculated and tabulated.

In vivo PDT Treatment of Subcutaneous PC3pip Tumors.

For *in vivo* PDT, 6−8-week-old male athymic nude mice were implanted subcutaneously with 1×10^6 GFP-expressing PC3pip cells. When the tumors were 4−6 mm in size, the animals received 0.07 mg/kg AuNP5kPEG-PSMA-1-Pc4 intravenously *via* tail-vein injection (based on Pc4 concentration). Three hours postinjection, the tumors were subjected to PDT treatment by irradiating the tumor using the same optical device described above. Detailed experimentation including calculations of fluence can be found in the Supporting Information. Three groups each having 5 mice were studied: (i) control/no treatment; (ii) AuNP5kPEG-PSMA-1-Pc4 + 150 J/cm^2; and (iii) AuNP5kPEG-PSMA-1-Pc4 + 300 J/cm^2. The mice were monitored for 14 days by measuring the tumor volume using a digital caliper, the GFP fluorescence by Maestro, and body weight.

Supplementary Material

Refer to Web version on PubMed Central for supplementary material.

ACKNOWLEDGMENTS

The authors gratefully acknowledge funding from the National Institutes of Health (Grant R01 EB020353–03). We also thank Dr. Afsana Akhter for performing the Western blot studies.

REFERENCES

(1). Siegel RL; Miller KD; Fedewa SA; Ahnen DJ; Meester RGS; Barzi A; Jemal A Colorectal Cancer Statistics, 2017. Ca-Cancer J. Clin 2017, 67, 177–193. [PubMed: 28248415]

(2). Jemal A; Siegel R; Ward E; Murray T; Xu J; Smigal C; Thun MJ Cancer Statistics, 2006. Ca-Cancer J. Clin 2006, 56, 106–130. [PubMed: 16514137]

(3). Momma T; Hamblin MR; Wu HC; Hasan T Photodynamic Therapy of Orthotopic Prostate Cancer with Benzoporphyrin Derivative: Local Control and Distant Metastasis. Cancer Res 1998, 58, 5425–5431. [PubMed: 9850075]

(4). Burnett AL; Aus G; Canby-Hagino ED; Cookson MS; D'Amico AV; Dmochowski RR; Eton DT; Forman JD; Goldenberg SL; Hernandez J; Higano CS; Kraus S; Liebert M; Moul JW; Tangen C; Thrasher JB; Thompson I American Urological Association Prostate Cancer Guideline Update, P., Erectile Function Outcome Reporting After Clinically Localized Prostate Cancer Treatment. J. Urol 2007, 178, 597–601. [PubMed: 17570435]

(5). Kundu SD; Roehl KA; Eggener SE; Antenor JA; Han M; Catalona WJ Potency, Continence and Complications in 3,477 Consecutive Radical Retropubic Prostatectomies. J. Urol 2004, 172, 2227–2231. [PubMed: 15538237]

(6). Penson DF; McLerran D; Feng Z; Li L; Albertsen PC; Gilliland FD; Hamilton A; Hoffman RM; Stephenson RA; Potosky AL; Stanford JL 5-Year Urinary and Sexual Outcomes After Radical Prostatectomy: Results From the Prostate Cancer Outcomes Study. J. Urol 2005, 173, 1701–1705. [PubMed: 15821561]

(7). Saranchuk JW; Kattan MW; Elkin E; Touijer AK; Scardino PT; Eastham JA Achieving Optimal Outcomes After Radical Prostatectomy. J. Clin. Oncol 2005, 23, 4146–4151. [PubMed: 15961762]

(8). Mhawech-Fauceglia P; Zhang S; Terracciano L; Sauter G; Chadhuri A; Herrmann FR; Penetrante R Prostate-Specific Membrane Antigen (PSMA) Protein Expression in Normal and Neoplastic Tissues and its Sensitivity and Specificity in Prostate Adenocarcinoma: an Immunohistochemical Study Using Mutiple Tumour Tissue Microarray Technique. Histopathology 2007, 50, 472–483. [PubMed: 17448023]

(9). Rauscher I; Maurer T; Fendler WP; Sommer WH; Schwaiger M; Eiber M (68)Ga-PSMA Ligand PET/CT in Patients with Prostate Cancer: How We Review and Report. Cancer Imaging 2016, 16, 14. [PubMed: 27277843]

(10). Chang SS Overview of Prostate-Specific Membrane Antigen. Rev. Urol 2004, 6, S13–8.

(11). Liu H; Rajasekaran AK; Moy P; Xia Y; Kim S; Navarro V; Rahmati R; Bander NH Constitutive and Antibody-Induced Internalization of Prostate-Specific Membrane Antigen. Cancer Res 1998, 58, 4055–4060. [PubMed: 9751609]

(12). Lucky SS; Soo KC; Zhang Y Nanoparticles in Photodynamic Therapy. Chem. Rev 2015, 115, 1990–2042. [PubMed: 25602130]

(13). Baron ED; Malbasa CL; Santo-Domingo D; Fu P; Miller JD; Hanneman KK; Hsia AH; Oleinick NL; Colussi VC; Cooper KD Silicon Phthalocyanine (Pc 4) Photodynamic Therapy is a Safe Modality for Cutaneous Neoplasms: Results of a Phase 1 Clinical Trial. Lasers Surg. Med 2010, 42, 728–735.

(14). Wang X; Tsui B; Ramamurthy G; Zhang P; Meyers J; Kenney ME; Kiechle J; Ponsky L; Basilion JP Theranostic Agents for Photodynamic Therapy of Prostate Cancer by Targeting Prostate-Specific Membrane Antigen. Mol. Cancer Ther 2016, 15, 1834–1844. [PubMed: 27297866]

(15). Meyers JD; Cheng Y; Broome AM; Agnes RS; Schluchter MD; Margevicius S; Wang X; Kenney ME; Burda C; Basilion JP Peptide-Targeted Gold Nanoparticles for Photo-dynamic Therapy of Brain Cancer. Part. Part. Syst. Charact 2015, 32, 448–457. [PubMed: 25999665]

(16). Cheng Y; Meyers JD; Broome AM; Kenney ME; Basilion JP; Burda C Deep Penetration of a PDT Drug into Tumors by Noncovalent Drug-Gold Nanoparticle Conjugates. J. Am. Chem. Soc 2011, 133, 2583–2591. [PubMed: 21294543]

(17). Cheng Y; Doane TL; Chuang CH; Ziady A; Burda C Near Infrared Light-Triggered Drug Generation and Release from Gold Nanoparticle Carriers for Photodynamic Therapy. Small 2014, 10, 1799–1804. [PubMed: 24515950]

(18). Cheng Y; Samia AC; Meyers JD; Panagopoulos I; Fei B; Burda C Highly Efficient Drug Delivery with Gold Nanoparticle Vectors for in vivo Photodynamic Therapy of Cancer. J. Am. Chem. Soc 2008, 130, 10643–10647. [PubMed: 18642918]

(19). Maeda H; Ueda M; Morinaga T; Matsumoto T Conjugation of Poly(styrene-co-maleic acid) Derivatives to the Antitumor Protein Neocarzinostatin: Pronounced Improvements in Pharmacological Properties. J. Med. Chem 1985, 28, 455–461. [PubMed: 3156994]

(20). Petros RA; DeSimone JM Strategies in the Design of Nanoparticles for Therapeutic Applications. Nat. Rev. Drug Discovery 2010, 9, 615–627. [PubMed: 20616808]

(21). Upreti M; Jyoti A; Sethi P Tumor Microenvironment and Nanotherapeutics. Transl Cancer Res 2013, 2, 309–319. [PubMed: 24634853]

(22). Nakamura Y; Mochida A; Choyke PL; Kobayashi H Nanodrug Delivery: Is the Enhanced Permeability and Retention Effect Sufficient for Curing Cancer? Bioconjugate Chem 2016, 27, 2225–2238.

(23). Bertrand N; Wu J; Xu X; Kamaly N; Farokhzad OC Cancer Nanotechnology: the Impact of Passive and Active Targeting in the Era of Modern Cancer Biology. Adv. Drug Delivery Rev 2014, 66, 2–25.

(24). Cheng Y; Meyers JD; Agnes RS; Doane TL; Kenney ME; Broome AM; Burda C; Basilion JP Addressing Brain Tumors with Targeted Gold Nanoparticles: A new Gold Standard for Hydrophobic Drug Delivery? Small 2011, 7, 2301–2306. [PubMed: 21630446]

(25). Banerjee SR; Foss CA; Horhota A; Pullambhatla M; McDonnell K; Zale S; Pomper MG 111In- and IRDye800CW-Labeled PLA-PEG Nanoparticle for Imaging Prostate-Specific Membrane Antigen-Expressing Tissues. Biomacromolecules 2017, 18, 201–209. [PubMed: 28001364]

(26). Von Hoff DD; Mita MM; Ramanathan RK; Weiss GJ; Mita AC; LoRusso PM; Burris HA, 3rd; Hart LL; Low SC; Parsons DM; Zale SE; Summa JM; Youssoufian H; Sachdev JC Phase I Study of PSMA-Targeted Docetaxel-Containing Nano-particle BIND-014 in Patients with Advanced Solid Tumors. Clin. Cancer Res 2016, 22, 3157–3163. [PubMed: 26847057]

(27). Zhang H; Liu X; Wu F; Qin F; Feng P; Xu T; Li X; Yang L A Novel Prostate-Specific Membrane-Antigen (PSMA) Targeted Micelle-Encapsulating Wogonin Inhibits Prostate Cancer Cell Proliferation via Inducing Intrinsic Apoptotic Pathway. Int. J. Mol. Sci 2016, 17, 676.

(28). Flores O; Santra S; Kaittanis C; Bassiouni R; Khaled AS; Khaled AR; Grimm J; Perez JM PSMA-Targeted Theranostic Nanocarrier for Prostate Cancer. Theranostics 2017, 7, 2477–2494. [PubMed: 28744329]

(29). Lee SS; Roche PJ; Giannopoulos PN; Mitmaker EJ; Tamilia M; Paliouras M; Trifiro MA Prostate-Specific Membrane Antigen-Directed Nanoparticle Targeting for Extreme Nearfield Ablation of Prostate Cancer Cells. Tumor Biol 2017, 39, 1–12.

(30). Nagesh PKB; Johnson NR; Boya VKN; Chowdhury P; Othman SF; Khalilzad-Sharghi V; Hafeez BB; Ganju A; Khan S; Behrman SW; Zafar N; Chauhan SC; Jaggi M; Yallapu MM PSMA Targeted Docetaxel-Loaded Superparamagnetic Iron Oxide Nanoparticles for Prostate Cancer. Colloids Surf., B 2016, 144, 8–20.

(31). Jazayeri MH; Amani H; Pourfatollah AA; Avan A; Ferns GA; Pazoki-Toroudi H Enhanced Detection Sensitivity of Prostate-Specific Antigen via PSA-Conjugated Gold Nanoparticles Based on Localized Surface Plasmon Resonance: GNP-coated anti-PSA/LSPR as a Novel Approach for the Identification of Prostate Anomalies. Cancer Gene Ther 2016, 23, 365–369. [PubMed: 27740614]

(32). Wang X; Huang SS; Heston WD; Guo H; Wang BC; Basilion JP Development of Targeted Near-Infrared Imaging Agents for Prostate Cancer. Mol. Cancer Ther 2014, 13, 2595–2606. [PubMed: 25239933]

(33). Doane TL; Cheng Y; Babar A; Hill RJ; Burda C Electrophoretic Mobilities of PEGylated Gold NPs. J. Am. Chem. Soc 2010, 132, 15624–15631. [PubMed: 20958038]

(34). Knop K; Hoogenboom R; Fischer D; Schubert US Poly(ethylene glycol) in Drug Delivery: Pros and Cons as well as Potential Alternatives. Angew. Chem., Int. Ed 2010, 49, 6288–6308.

(35). Tsubone T; Braga G; Vilsinki B; Gerola A; Hioka N; Tessaro A; Caetano W Aggregation of aluminum phthalocyanine hydroxide in water/ethanol mixtures. J. Braz. Chem. Soc 2014, 25, 890–897.

(36). Yoon M; Cheon Y; Kim D Absoprtion and Fluorescence Spectroscopic Studies on Dimerization of Chloroaluminum (III) Phthalocyanine Tetrasulfonate in Aqueous Alcoholic Solutions. Photochem. Photobiol 1993, 58, 31–36.

(37). Kobayashi H; Watanabe R; Choyke PL Improving Conventional Enhanced Permeability and Retention (EPR) Effects; What is the Appropriate Target? Theranostics 2013, 4, 81–89. [PubMed: 24396516]

(38). Pielichowski K; Flejtuch K Differential Scanning Calorimetry Studies on Poly(ethylene glycol) with Different Molecular Weights for Thermal Energy Storage Materials. Polym. Adv. Technol 2002, 13, 690–696.

(39). Hong S; Leroueil PR; Majoros IJ; Orr BG; Baker JR, Jr. Banaszak Holl MM, The Binding Avidity of a Nanoparticle-based Multivalent Targeted Drug Delivery platform. Chem. Biol 2007, 14, 107–115. [PubMed: 17254956]

(40). Tassa C; Duffner JL; Lewis TA; Weissleder R; Schreiber SL; Koehler AN; Shaw SY Binding Affinity and Kinetic Analysis of Targeted Small Molecule-Modified Nanoparticles. Bioconjugate Chem 2010, 21, 14–19.

(41). Halliwell B; Whiteman M Measuring Reactive Species and Oxidative Damage in vivo and in Cell Culture: How Should You Do It and What Do the Results Mean? Br. J. Pharmacol 2004, 142, 231–255. [PubMed: 15155533]

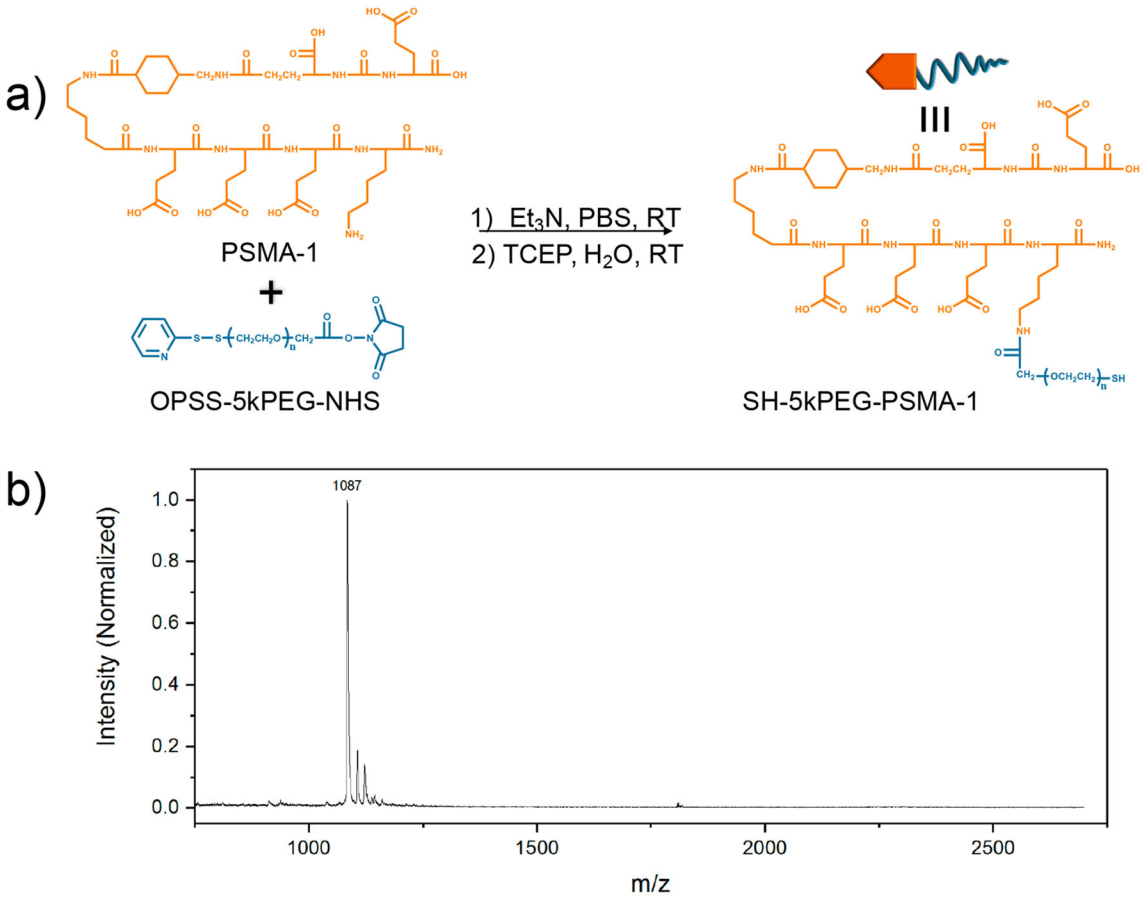

Figure 1.

(a) Conjugation of PSMA-1 to OPSS-5kPEG-NHS followed by deprotection of thiol and (b) MALDI-TOF mass spectra of PSMA-1.

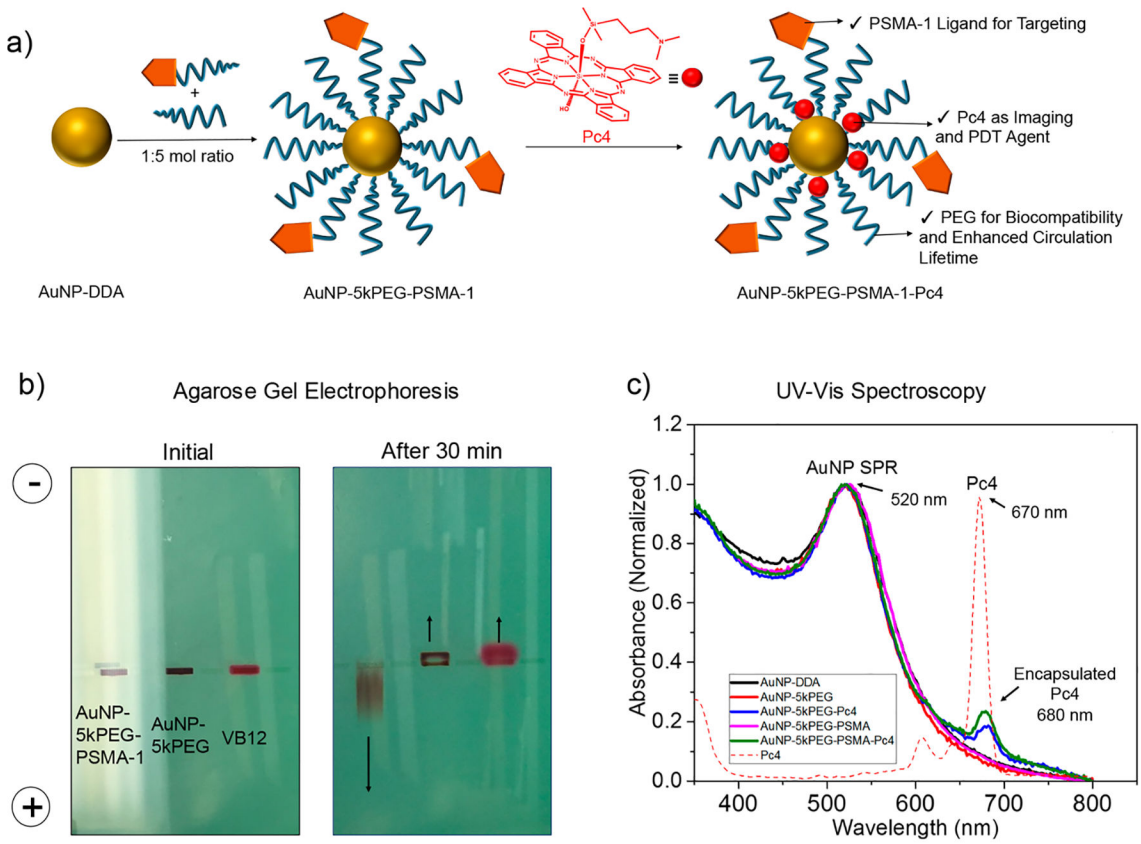

Figure 2.

(a) Synthesis of AuNP-5kPEG-PSMA-1 and loading of Pc4. (b) Agarose gel electrophoresis demonstrates the successful binding of 5kPEG-PSMA-1 to AuNP (c) UV−vis absorbance spectroscopy shows that Pc4 is incorporated into the nanoparticle system.

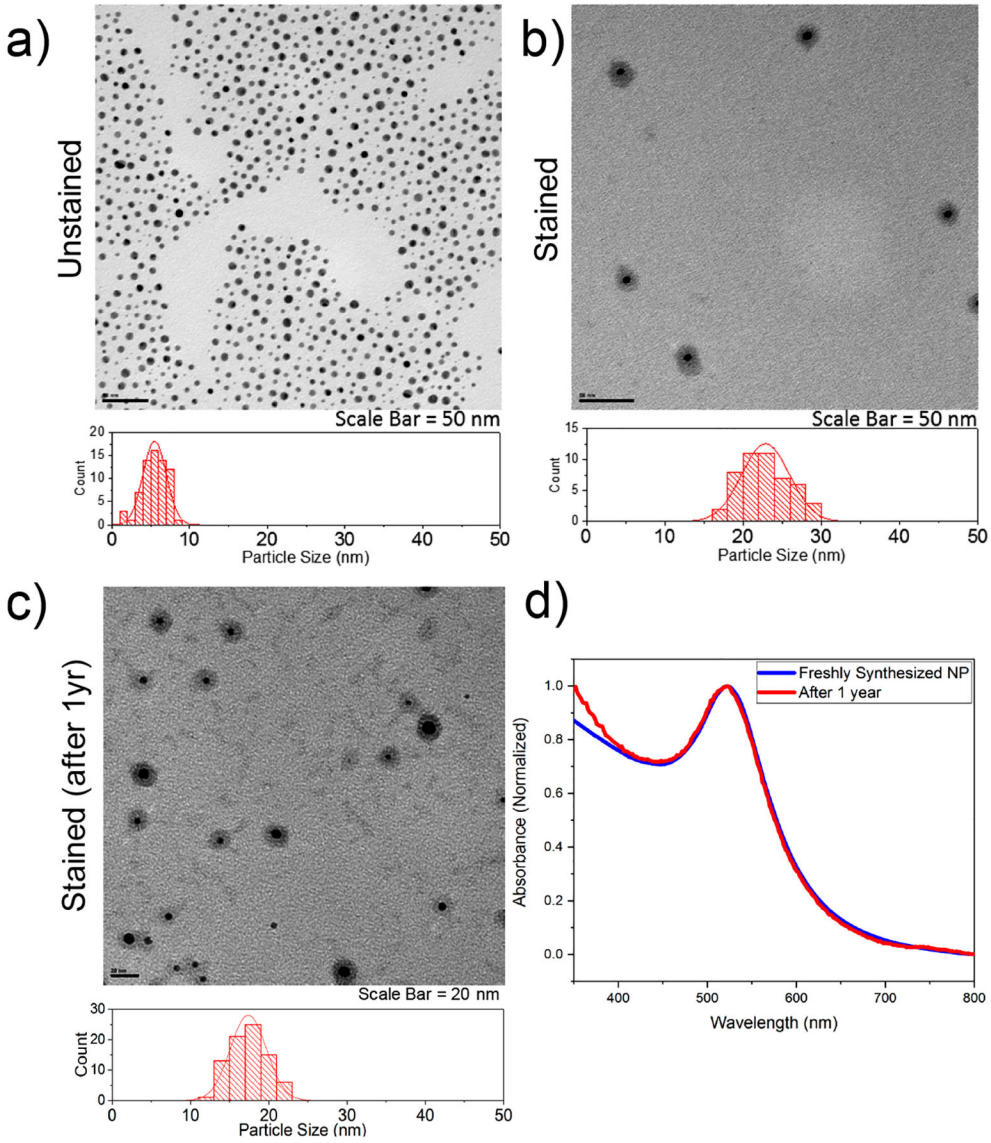

Figure 3.

Transmission electron microscopy of (a) unstained and (b) stained AuNP conjugates evidenced the formation of fairly monodispersed nanoparticles. (c) TEM image and (d) UV −vis spectra of the same nanoparticle after one year of storage at −20 °C.

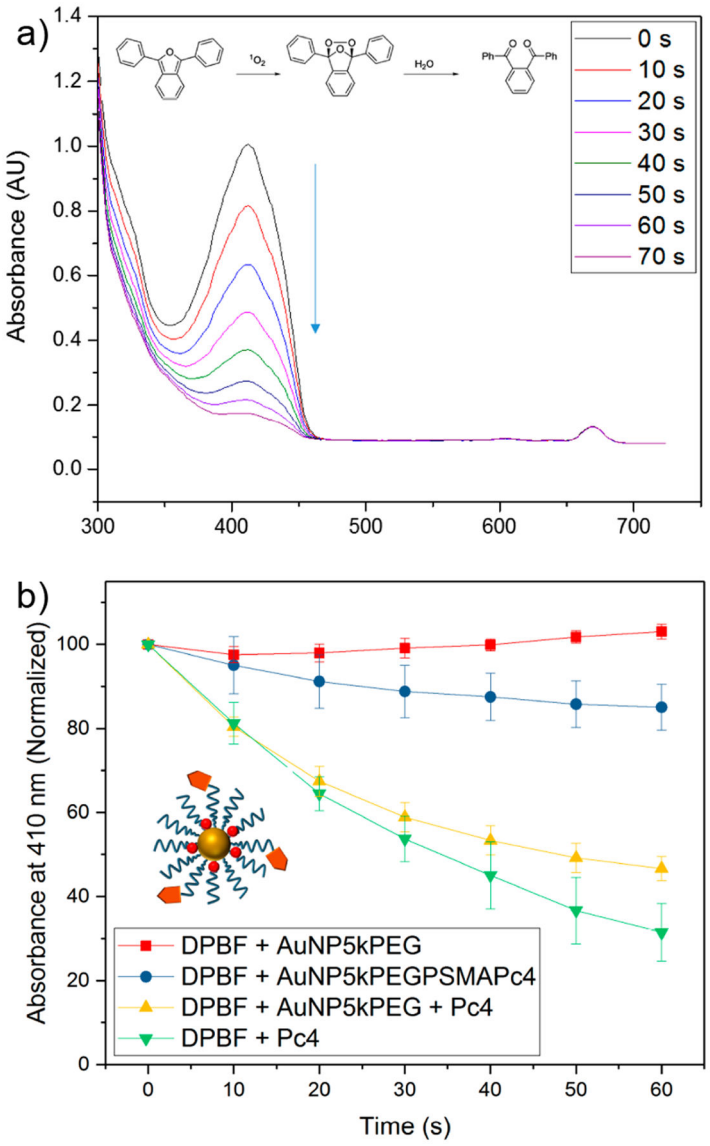

Figure 4.

(a) $^1O_2$ generation was confirmed by monitoring the oxidation of a singlet oxygen trap, diphenylisobenzofuran (DPBF). The inset shows the chemical transformation of DPBF in the presence of $^1O_2$. (b) Evaluation of $^1O_2$ generation of Pc4 in gold nanoparticles in EtOH solution. The data suggest that Pc4 molecules are indeed trapped in the polymer shell of the AuNP.

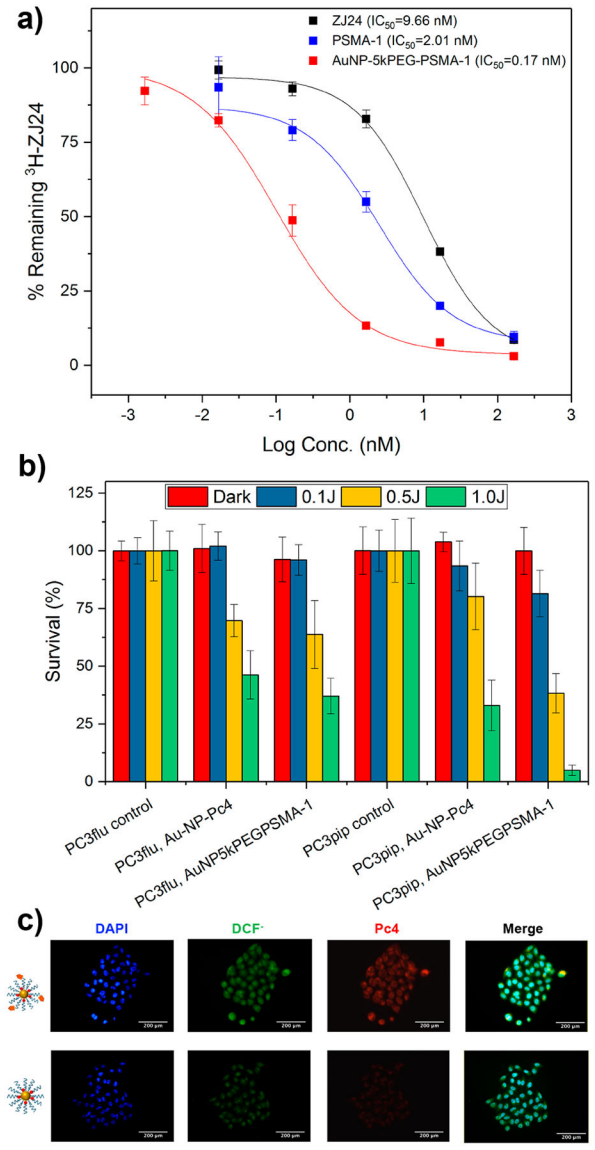

Figure 5.

(a) Competition binding study for different PSMA ligands: parent ZJ24, PSMA-1, and AuNP5kPEGPSMA-1. (b) Efficacy of AuNP-5kPEG-PSMA-1-Pc4 for killing prostate cancer cell lines. (c) Results of a DCFDA assay showing fluorescence images of PC3pip cells postirradiation (scale bar = 200 μm). Error bars ± SD.

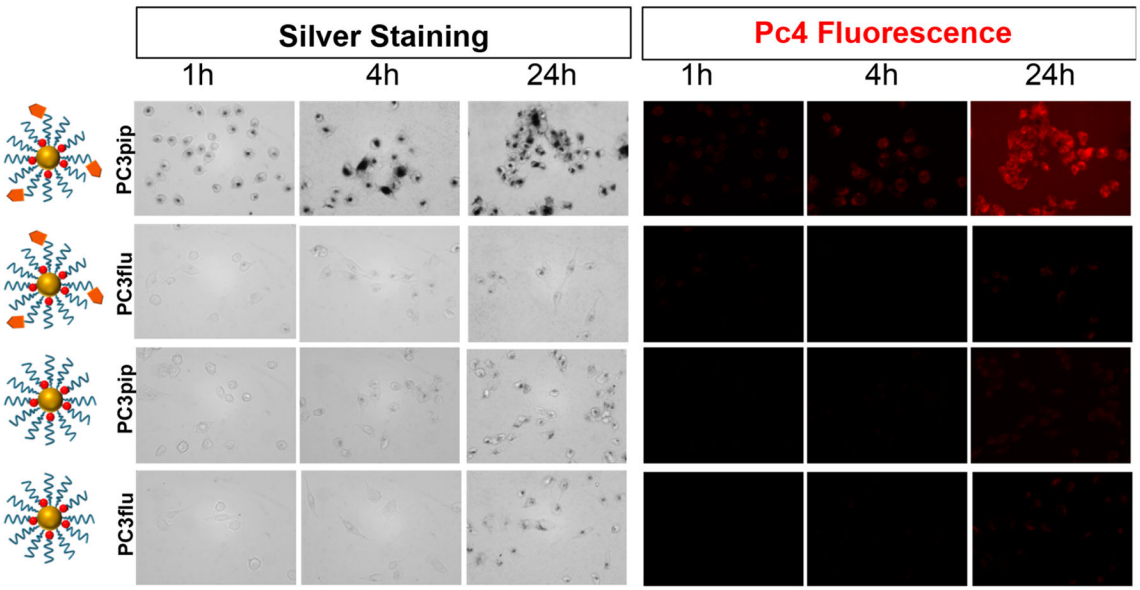

Figure 6.

Cellular uptake study of targeted and nontargeted AuNP. Pc4 fluorescence was visualized using a fluorescence microscope, and Au nanoparticles were visualized using white light after enhancement with silver staining (dimension = 853 × 638 μm). Images were taken at 400×.

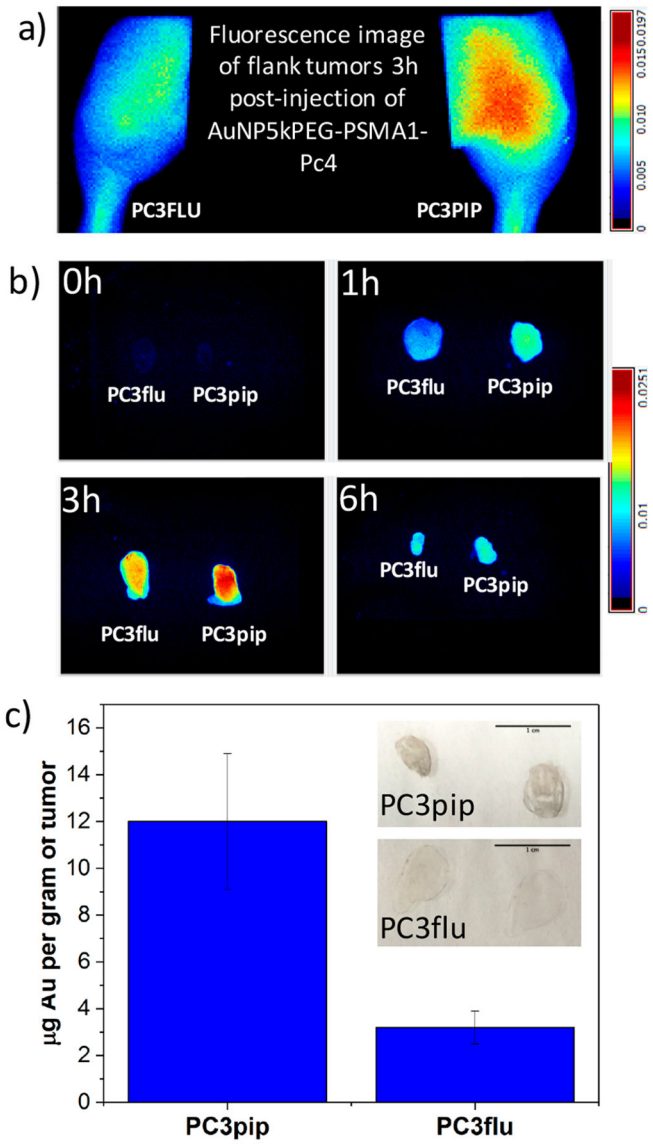

Figure 7.

(a, b) Maestro fluorescence images showing selective accumulation of AuNP-5kPEG-PSMA-1-Pc4 on PC3pip tumor. (c) Gold content of excised PC3pip and PC3flu tumors 3 h postinjection of AuNP-5kPEG-PSMA-1-Pc4 and (inset) sections of PC3pip and PC3flu stained with silver (scale bar = 1 cm).

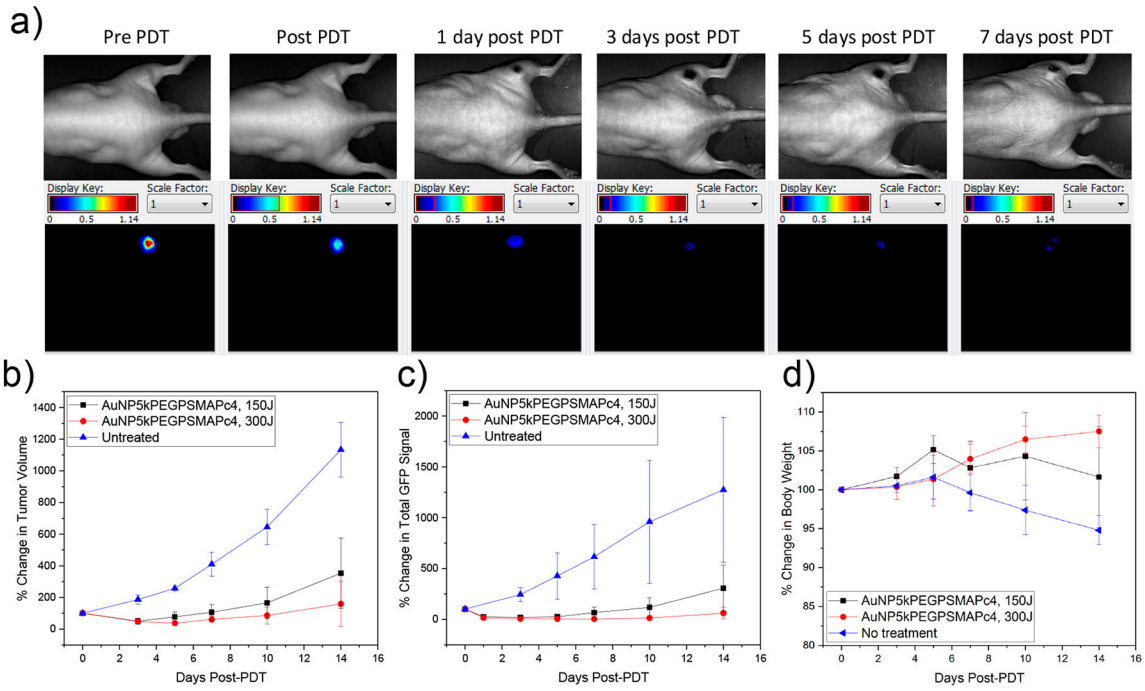

Figure 8.

(a) Representative images of the same mouse monitored for GFP fluorescence after receiving 0.07 mg/kg AuNP-5kPEG-PSMA-1-Pc4 followed by PDT (300 J/cm^2). The efficacy of the treatment was determined by monitoring (b) tumor volume, (c) total GFP signal, and (d) body weight (n = 5).

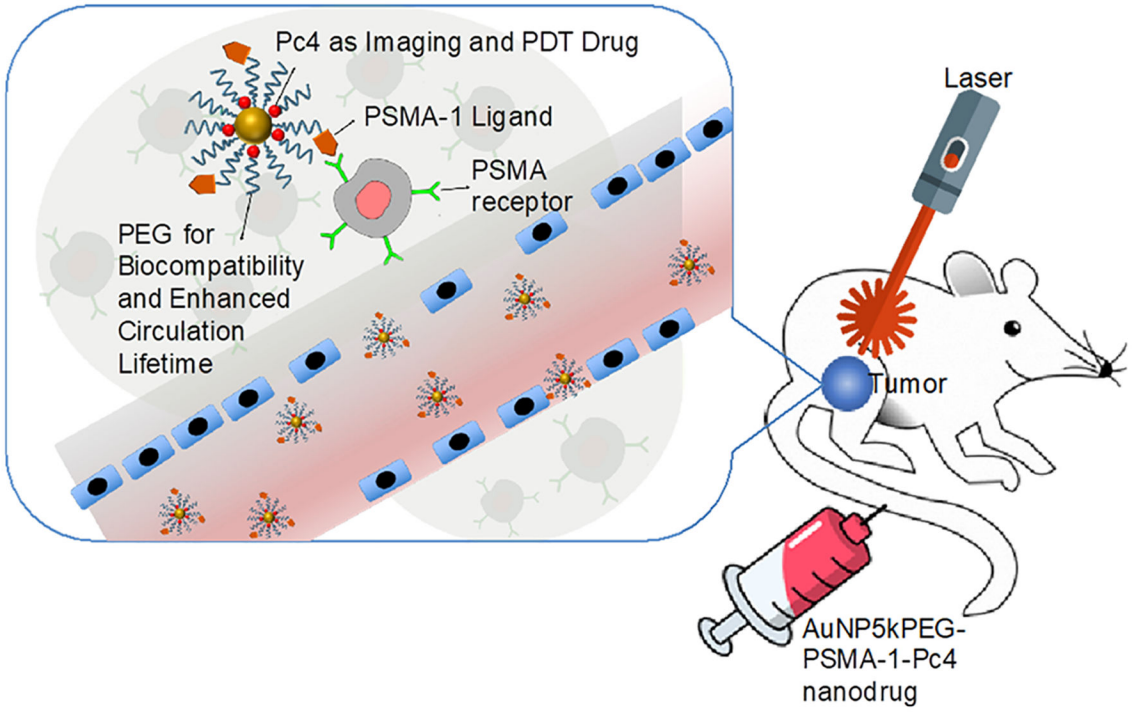

Scheme 1.
Design of PSMA-1-targeted gold nanoparticles containing Pc4 as imaging and PDT agent.